Article

A Strategy for In-Situ Imaging of Cellular Alkaline Phosphatase Activity Using Gold Nanoflower Probe and Localized Surface Plasmon Resonance Technique

Kan Wang, Ling Jiang, Fen Zhang, Yuanqing Wei, Kang Wang, Huaisheng Wang, Zhengjian Qi, and Songqin Liu

Anal. Chem., **Just Accepted Manuscript** • DOI: 10.1021/acs.analchem.8b04179 • Publication Date (Web): 08 Nov 2018

A Strategy for *In-Situ* Imaging of Cellular Alkaline Phosphatase Activity Using Gold Nanoflower Probe and Localized Surface Plasmon Resonance Technique

Kan Wang,[†] Ling Jiang,[†] Fen Zhang,[†] Yuanqing Wei,[†] Kang Wang,[*‡] Huaisheng Wang,[#] Zhengjian Qi,[†] and Songqin Liu[*†]

[†]State Key Laboratory of Bioelectronics, Jiangsu Engineering Laboratory of Smart Carbon-Rich Materials and Device, School of Chemistry and Chemical Engineering, Southeast University, Nanjing, 211189, People's Republic of China

[‡]State Key Laboratory of Analytical Chemistry for Life Science and Collaborative Innovation Center of Chemistry for Life Sciences, School of Chemistry and Chemical Engineering, Nanjing University, Nanjing 210093, People's Republic of China

[#]Department of Chemistry, Liaocheng University, Liaocheng, Shandong, 252059, China

[*]Corresponding author: Tel.: 86-25-52090613; Fax: 86-25-52091098. E-mail: liusq@seu.edu.cn (S.Q. Liu); wangkang@nju.edu.cn (K. Wang)

ABSTRACT

In this work, a simple and ultrasensitive localized surface plasmon resonance (LSPR) method that use Au nanoflowers (AuNFs) as probe was designed for *in-situ* monitoring of alkaline phosphatase (ALP) activity. The AuNFs was fabricated by hydrogen tetrechloroaurate-induced oxidative disruption of polydopamine-coated Au nanoparticles (AuNPs) and subsequently growth of Au nanopetals on AuNPs. The as-prepared AuNFs showed a much higher LSPR capability and stronger scattering color change than AuNPs. The strategy for *in-situ* cellular ALP activity detection relied on the deposition of Ag on AuNFs surface, which changed the morphology of AuNFs and led to a tremendous LSPR response and scattering color change. The deposition of Ag shell on AuNFs was related to ALP activity, where ALP catalyzed the hydrolysis of L-ascorbic acid 2-phosphate sesquimagnesium salt hydrate to form L-ascorbic acid (AA), then AA reduced Ag^{+} to Ag and deposited onto AuNFs. With this concept, the ALP activity could be monitored with a detection limit of 0.03 μU L^{-1}. Meanwhile, the ALP activity of single HepG2 cells and HEK 293 cells was tracked with proposed approach, which indicated the trace expression level of ALP in HEK 293T cell and overexpressed level of ALP in HepG2 cells. After treated with drugs, the cellular ALP activity of HepG2 cells was decreased with the treating time and dose increasing. Therefore, the proposed strategy could be used for tracking the cellular ALP activity, which paved a new avenue for cell studies, and hold great potential for discovering novel ALP-based drugs applications.

INTRODUCTION

Alkaline phosphatase (ALP), an essential zinc-containing dimeric enzyme that responsible for phosphate metabolism and catalyzed the hydrolysis of phosphoryl esters in alkaline media, is widely distributed in several tissues throughout the body, particularly concentrated in the bone and liver.[1-3] Abnormally elevation of ALP activity in blood is commonly linked to various diseases such as liver diseases and bone disorders.[4,5] While low activity of ALP in blood is the sign of hypophosphatasia and some other diseases such as anemia and chronic nephritis.[6] Meanwhile, the ALP activity fluctuates with many cellular events, including transformation, response to toxic injury and tumor aggressiveness.[7,8] Notably, cellular ALP are overexpressed in some malignant tumors, which can be further implicated as a tumor biomarker.[9-11] Therefore, the ALP is an important biomarker for clinical diagnosis, and tracking of ALP activity at cellular level provides valuable information on the cell differentiation and viability to identify the abnormality in cell behaviors.[12-14] To date, numbers of approaches have been developed to monitor ALP activity including chromatography,[15] electrochemistry,[16] surface-enhanced resonance Raman scattering,[17] fluorescence spectra and colorimetry.[18-20] For example, You and co-workers proposed a new inner filter effect-based fluorescent assay for ALP sensing, ALP inhibitor investigation and cell imaging, in which N-doped carbon dots act as fluorophore and the hydrolysate of ALP as absorber. [19] With the color change of the enzyme-assisted silver deposition on the gold nanorod, Tang and co-workers developed a colorimetric approach for semi-quantify the ALP activity in serum.[20]

Although these methods have enabled high sensitivity, good selectivity, label-free and simple detection of ALP activity, the incapability of these methods for imaging in live cells and relatively low sensitivity at cell level limit their practical applications.

Recently, the label-free localized surface plasmon resonance (LSPR) detection technique has been developed for *in-situ* biological detection and cell imaging.[21-27] The LSPR signal comes from the coherent oscillation of the conduction electrons in the conduction band of plasmonic nanoparticles.[28-30] The scattering light of an individual plasmonic nanoparticle can be observed at single particle level under a dark-field microscope, providing much improved spatiotemporal resolution than the traditional averaged measurement.[31-33] Additionally, LSPR signal mainly depends on the nanoparticle morphology, size, composition, as well as surrounding dielectric environment.[34-38] Therefore, efforts toward the development of plasmonic nanoparticles with different shapes and architectures such as nanoflowers, nanorods, nanocubes and core-satellites nanostructures have been made to enhance the scattering spectral shift, which are more sensitive to the change of the interface micro-environment on nanoparticle surface.[39-45] For example, Wang and co-workers designed a smart plasmonic nanobiosensor based on individual Au@Ag core-shell nanocube modified with tetrahedron-structured DNA for detecting microRNA 21 at the single-molecule level.[40] Yeung and co-workers introduced a Au-Ag core-shell nanorods as probe for highly sensitive sulphide mapping in live cells based on the Ag_2S formation.[41] Our previous work designed a core–satellites nanostructure of $Au_{50}@Au_{13}$ probe for label-free LSPR sensing and cellular imaging of telomerase

activity. The telomerase-triggered disassembly of $Au_{50}@Au_{13}$ could be observed by amplified LSPR spectral shift accompanied by color changes from orange to green.[42]

Inspired by very promising applications of the plasmonic nanoparticles in LSPR sensing and cell imaging, herein, a monodispersed Au nanoflowers (AuNFs) with branched Au nanopetal structure was synthesized and used as LSPR probe for *in-situ* monitoring the ALP activity and cellular ALP imaging. The cellular ALP activity detection was relied on the deposition of Ag on AuNFs surface, which changed the morphology of AuNFs and led to a tremendous LSPR peak blue shift along with a scattering color change from red to green. The formation of Ag shell on AuNFs surface was related to ALP activity, where ALP catalyzed the hydrolysis of L-ascorbic acid 2-phosphate sesquimagnesium salt hydrate (AAP) to form L-ascorbic acid (AA), then AA reduced Ag^+ to Ag and deposited onto AuNFs. With this concept, we could *in-situ* and undamaged monitoring of cellular ALP activity in living cells (Scheme 1).

EXPERIMENTAL SECTION

Preparation of Gold Nanoflowers. Gold nanoparticles **(**AuNPs) with diameter of 13 nm (Au_{13}) were synthesized by trisodium citrate reduction method.[46] AuNPs with diameter of 50 nm (Au_{50}) were prepared by using seed-growth method.[47] Briefly, 25 mL of ultrapure water, 1 mL of Au_{13} (used as seed), and 400 μL of 0.2 M $NH_2OH{\cdot}HCl$ solution were sequentially injected in a 50 mL beaker. Then 4 mL of 0.2 wt% $HAuCl_4$ was added dropwise to the mixture under vigorous stirring for 30 min at room temperature. Au_{50} was thus obtained and stored in dark beaker at 4 °C. The

concentration of the Au_{50} solution was calculated to 0.1 nM, using the Lambert–Beer law with the extinction coefficient of 1.5×10^{10} $M^{-1}cm^{-1}$.[48]

1 mL of the above prepared Au_{50} was centrifuged and re-dispersed in pH 8.5, 10 mM Tris buffer to final volume of 1 mL. Then, 5 μL of 0.5 mg mL^{-1} dopamine·HCl solution in 10 mM pH 8.5 Tris buffer was added, and the reaction mixture was vortexed at 25 °C for 4 h. Finally, the reaction mixture was centrifuged at 6000 rpm for 5 min, the polydopamine-coated Au_{50} (PDA/Au_{50}) was obtained and re-dispersed in ultrapure water to a final volume of 1 mL.

For the synthesis of AuNFs, 1 mL of above PDA/Au_{50} solution, 150 μL of 5 mM $HAuCl_4$, 100 μL of 5% w/v polyvinylpyrrolidone (PVP) (10,000 MW), and 150 μL of 50 mM hydroxyl amine were added consecutively, and the reaction mixture was rigorously shaken for 5 min at 25 °C. After centrifugation at 6000 rpm for 5 min and washing with ultrapure water several times, the obtained AuNFs were dispersed in 1 mL of ultrapure water and stored at 4 °C for future uses.

Detection of ALP Activity *in vitro*. Prior to ALP activity detection, cleaned glass slides were treated with 1% (v/v) aqueous solution of 3-aminopropyl-trimethoxysilane (APTS) for 1 h. Then, it was washed with ultrapure water and ethanol for several times, dried under N_2 flow and baked at 110 °C for 30 min. The glass slides that modify with amino-group were thus obtained.

100 μL of diluted AuNFs (1 pM) was dropped onto the amino-functionalized glass slide and incubated for 4 min. Then, the glass slide was washed with ultrapure water and dried with N_2 stream. For the *in vitro* monitoring of ALP, 200 μL of Tris buffer

(pH 8.5) containing 0.01 μM $AgNO_3$, 0.02 μM AAP and various concentrations of ALP were added and incubated at 37 °C for 30 min. The ALP activity was evaluated by the dark-field measurements based on the LSPR shift induced by ALP guided silver growth on individual AuNFs.

The AuNFs were also used to detect the diluted real human blood samples with the same way, and compared the detection results with clinic method measured with commercial ELISA kit. Human blood samples were collected from the Hospital of Southeast University.

Cell culture and Cellular ALP imaging. Cells were cultured in Dulbecco's modified Eagle's medium (DMEM, GIBCO) supplemented with 15% fetal calf serum (FCS, Sigma), penicillin (100 μg mL^{-1}), and streptomycin (100 μg mL^{-1}) in 5% CO_2, 37 °C incubator. The cell number was determined with a cell-counting board.

For cellular imaging of ALP activity with AuNFs probe, 200 μL of HepG2 cells (5×10^3 cells mL^{-1}) were seeded in each confocal dish and cultured for 12 h. Then 50 μL of AuNFs was added into the dish and incubated at 37 °C for 30 min. DFM images were collected after the dish was washed with PBS buffer (pH 7.4) and immersed in 200 μL of Tris buffer (pH 8.5) buffer containing 2.5 μM $AgNO_3$, 5 μM AAP for DFM imaging. To test the effect of drugs on cellular ALP activity, 200 μL of HepG2 cells (5×10^3 cells mL^{-1}) were cultured with different amounts of Na_3VO_4 in confocal dish for 12 h. Then DFM imaging and scattering spectra scanning were collected according to above mentioned method.

Cell Viability Assay. For cell viability assay, HepG2 cells were seeded and cultured

for 48 h in 96-well plates. Then 50 μL of AuNFs was added to each well and incubated for different times, followed by addition of 50 μL MTT solution (1 mg mL^{-1}) and incubation at 37 °C for 4 h. After that, 100 μL of dimethyl sulphoxide was added and vibrated for 15 min, the absorbance at a wavelength of 490 nm was measured to obtain the cell viability using a microplate reader. Details and the further experimental measurements can be found in the Supporting Information "Materials and Methods".

RESULTS AND DISCUSSION

Characterization of AuNFs probe. AuNPs with average diameters of 50 nm were synthesized by seed-growth method. Then the as-prepared Au_{50} were treated with dopamine to cover a highly cross-linked polydopamine (PDA) layer on Au_{50} through a Tris-initiated consecutive oxidation, intramolecular cyclization, and oligomerization under alkaline conditions.[49] The SEM images showed that the resulting PDA/Au_{50} was well monodispersed, and the thickness of PDA membrane increased from 5 nm to 30 nm depending on the concentration of dopamine after 4 h reaction (Figure S1). The catechol moieties of PDA can be oxidized by $HAuCl_4$, which cause the disruption and degradation of the PDA layer, thus facilitating the subsequent growth and deposition of Au petal nanostructures on Au_{50} core.[50] In our experiments, thicker PDA layer on Au_{50} resulted in low degree of petal protrusion on Au_{50}. Therefore, PDA/Au_{50} with 5 nm of PDA layer was used for the synthesis of AuNFs. TEM images of the resulting AuNFs showed a distinct morphological change where the massively branched nanopetals were grown on round AuNPs. With the increase of $HAuCl_4$, the surface of

Au_{50} core varied gradually from smooth to rough (Figure S2). When $HAuCl_4$ concentration reached to 0.5 mM, both TEM and SEM images revealed that the obtained AuNFs displayed good monodispersity and uniform sizes with highly branched petals structure on spherical AuNPs core (Figure S3). Therefore, 0.5 mM of $HAuCl_4$ concentration was chosen as optimal concentration for the formation of AuNFs.

The as-prepared AuNFs with blue color displayed a maximum extinction peak at 590 nm, which was about 60 nm red shifted comparing to Au_{50} with red color for the strong plasmonic couplings between closely positioned metal nanopetals of AuNFs. The corresponding DFM and LSPR response of an individual AuNPs and AuNFs on glass slide showed that AuNFs scattered red light with LSPR peak centered at 655 nm because of the dielectric constant of glasss slide is bigger than water, while AuNPs scattered green light with LSPR peak centered at 565 nm (Figure 1). The LSPR peak shift between AuNFs and AuNPs was about 90 nm. The dynamic light scattering (DLS) measurements showed that the AuNFs had an average hydrodynamic diameter abound 65 nm. The 15 nm increasement in diameter was contributed to the formation of branched nanopetals on AuNPs core (Figure S4). All these observations demonstrated the successful formation of AuNFs.

Detection of ALP Activity with AuNFs. AuNFs was used for ALP activity analysis based on the ALP-triggered Ag^+ depositing. After incubation of AuNFs in Tris buffer containing $AgNO_3$, AAP and ALP, both SEM and TEM images showed that the original petal protrusion of AuNFs gradually disappeared and even formed a

sphere-like nanostructure at the high ALP concentration in the incubation solution (Figure 1, S5 and S6). The corresponding EDS spectra showed the presence of Ag element on AuNFs (Figure S7). However, when AuNFs was incubated in a mixture without any component of ALP, AAP or $AgNO_3$, no obviously morphological changes were observed on AuNFs. We then contribute the changing of AuNFs morphology to the formation of Ag shell on AuNFs (AuNF@Ag). As shown in Scheme 1, the ALP catalyzed hydrolysis of AAP to produce AA, then AA reduced Ag^+ to Ag on the surface of AuNFs. The similar phenomenon was also observed on AuNPs at the same conditions as AuNFs, however, the size of the as-produced nanosphere for AuNPs were much smaller than that of AuNFs (Figure S8). The formation of AuNF@Ag led the LSPR spectrum of AuNFs blue-shift and the scattering color changed from red to green (Figure 1). Meanwhile, both LSPR blue-shift and scattering color changing were proportioned with the extent of Ag^+ deposition on the surface of AuNFs, which thus related to the activity of ALP.

The dose-dependent response of ALP activity to Ag^+ deposition on AuNFs was investigated by DFM images and corresponding scattering spectra. Notably, with the increase of ALP activity, the scattering color of AuNFs gradually changed from red to yellow, and finally to green (Figure S9). Simultaneously, the LSPR peak of an individual AuNFs blue shifted from ~655 nm to ~565 nm, the remarkable peak shifts and scattering color changes were sufficient to identify the activity of ALP by using an individual AuNFs (Figure 2A). The linear response range of LSPR peak shift to the logarithm of ALP activity was from 0.1 to 60 μU L^{-1} with a detection limit of 0.03 μU

L^{-1} (S/N=3, Figure 2B). The linear equation could be represented by $y = 34.538 + 32.945 \log(x)$ with $R^2 = 0.996$, where y and x were the LSPR peak shift of AuNFs and ALP activity, respectively.

At a certain concentration of ALP, the time-dependent of LSPR peak shifts were drastically increased with an increasing reaction time, and reached a maximum value at 30 min (Figure 3A). In contrast, the LSPR peak shifts of AuNPs core reached a maximum value at around 60 min, indicating that AuNFs probe could greatly enhance the signal intensity and the rate of ALP catalytically reaction. The dose-dependent response of ALP activity to Ag^+ deposition on the AuNPs was also observed. But the LSPR peak shift on AuNPs was much smaller than that on AuNFs (Figure 3B). The ALP-triggered Ag^+ deposition on the AuNFs led a maximum LSPR peak shift of 90 nm, which was larger than that of 55 nm for AuNPs core. Meanwhile, with increasing of the ALP activity, the scattering color of an individual AuNPs was hardly to be distinguished (Figure S10). All these results confirmed that the ALP-triggered Ag^+ deposition on the AuNFs enabled to monitor ALP activity in single particle level with better analytical performance than that of AuNPs, including the short time-dependent, large LSPR peak shift and distinguished color changing.

To explore the selectivity of the ALP-triggered Ag^+ deposition, bovine serum albumin (BSA), thrombin (Thr), glucose oxidase (GOX), and glucose dehydrogenase (GDH) were used to replace ALP in the incubation of AuNFs solution containing AAP and $AgNO_3$, respectively. Only small LSPR peak shifts (less than 3 nm) were obtained for BSA, Thr, GOX, and GDH, respectively, confirming good selectivity of

the ALP-triggered silver deposition (Figure 3C). In addition, the hydrolysis activity of ALP could be greatly inhibited by drugs, chemicals and so on. Sodium orthovanadate (Na_3VO_4) was used as a model chemical for ALP inhibitor screening assays. The dose-dependent study showed that the ALP activities were dramatically decreased upon addition of Na_3VO_4 at a low concentration. About 90% ALP activity was inhabited when Na_3VO_4 concentration was rose to 0.2 nM, confirming the successful inhibitation of the hydrolysis activity of ALP by Na_3VO_4 (Figure 3D). The half maximal inhibitory concentration (IC_{50}) was estimated to be 4.6 pM for Na_3VO_4, which was consistent with previous reports.[2]

To assess the reliability of the developed ALP sensing method, ALP activity was test by standard addition approach in three serum samples achieved from the health donor in the Hospital of Southeast University. The results in Table S1 showed that the recoveries varied from 94% to 97% with the relative standard deviation (RSD) less than 5.4%, indicating a good feasibility for detecting ALP in human serum. The proposed LSPR method was also used to detect ALP activity in real human serum samples, and compared with a commercial ELISA method. As shown in Table S2, the results obtained from LSPR method were consistent well with those obtained from the ELISA method. The acceptable recovery and high accuracy indicated a great potential that the proposed ALP-triggered silver deposition sensing method could be used for ALP determination in real samples.

***In-situ* imaging of ALP in living cell.** HepG2 cells were selected as model cell lines for the living cell analysis because of their overexpressed ALP. Prior to cell imaging,

the cytotoxicity of AuNFs was examined by MTT assay. The HepG2 cells maintained more than 97 % of cell viabilities after incubation only with AuNFs for 4 h. In the presence of 0.25 pM AuNFs, 2.5 nM $AgNO_3$ and 5 nM AAP, the HepG2 cells maintained more than 93 % of cell viabilities, which was slightly deceased by using only AuNFs (Figure S11). In addition, the HepG2 cells viabilities were still more than 87% with 100-fold higher concentrations of AuNFs (25 pM), $AgNO_3$ (0.25 μM) and AAP (0.5 μM) (Figure S12). Therefore, the AuNFs had good biocompatibility and negligible cytotoxic effect, which could be used for *in-situ* monitoring of ALP activity in living cell.

The ALP activity in HepG2 cells was analyzed by DFM imaging and scattering spectra scanning with AuNFs as probe. The optimal concentrations of AuNFs and incubation time with HepG2 cells were selected to be 0.25 pM and 30 min, which were suitable for further cell analysis at single particle level (Figure S13 and S14). In addition, no obvious scattering changes of AuNFs probes were observed after HEK 293T cells treated with AuNFs and Ag^+ (without AAP), indicating the good selectivity and the significance of ALP catalyzed hydrolysis of AAP to produce reducing AA (Figure S15). After incubation of AuNFs with HepG2 cells for 30 min, several red scattering light spots corresponding to the AuNFs probes were observed on a single HepG2 cell (Figure 4A). The scattering signal of a single AuNFs probe was much stronger than the background scattering signal of the cell, making it a high resolution in living cell analysis. The scattering spectrum of three AuNFs probe (marked by red circles) was measured and the LSPR peak was about 655 nm. After

DFM imaging and scattering spectra scanning measurements, the slide was immersing in Tris buffer (10 mM, pH 8.5) buffer containing 2.5 nM $AgNO_3$ and 5 nM AAP. With increasing of the incubation time to 30 min, the scattered light of the AuNFs on the cell gradually turned into orange, yellow and green (Figure 4B-D). Meanwhile, scattering spectra of the selected three probes displayed notable spectral blue-shift as time elapsed, the LSPR peak of an individual AuNFs changed from 655 nm to 622, 584 and 570 nm for incubation of 10, 20, 30 min, respectively (Figure. 4E and F). Both LSPR peak shift and scattering color changing indicated the feasibility of AuNFs probe for *in-situ* imaging of ALP activity in living cell at signal particle level.

To test the cancer cell resolution, HEK 293 cells were used as phosphatase negative controls.[12] As shown in the DFM images, the AuNFs probes exhibited apparent scattering color changes from red to green after HepG2 cells treated with AuNFs, Ag^+ and AAP (Figure 5A and B). In contrast, no obvious scattering changes of AuNFs probes were observed at the membrane of HEK 293T cells under the same conditions, indicating the trace expression level of ALP in HEK 293T cell and the significance of ALP for Ag^+ deposition on AuNFs (Figure 5C and D). The ALP activity of single HepG2 cells and HEK 293 cells were calculated to be 6.8 and 0.6 pU $cell^{-1}$ based on the linear equation between the LSPR peak shift of AuNFs and the ALP activity. The AuNFs was further employed for monitoring the variation of cellular ALP activity after treated with drugs. The dose-dependent inhibition of ALP activity was certified by using HepG2 cells and Na_3VO_4. HepG2 cells were cultured with 0.25 pM AuNFs and different amounts of Na_3VO_4 (0, 20, 100 and 200 nM), all

AuNFs located at the cell membrane had red color with LSPR peak at ~655 nm (Figure 5E, G, I and K). After incubated with Ag^+ and AAP, the scattering color of AuNFs changed from green to red with increasing doses of Na_3VO_4 from 0 to 200 nM, and the LSPR peak gradually red shifted from 570 nm to 646 nm, which indicated a decrease of ALP activity in the HepG2 cells (Figure 5F, H, J and L). The corresponding ALP activity of single HepG2 cells treated with different amounts of Na_3VO_4 were estimated to be 6.8, 3.8, 1.6, and 0.04 pU $cell^{-1}$, respectively. Therefore, the AuNFs probe provided a potential tool for undamaged monitoring of ALP activity and discovering of new ALP-related drugs.

CONCLUSIONS

In summary, this work designed a novel label-free method for ultrasensitive detection of ALP activity based on AuNFs probe and LSPR technique. The densely protruding nanopetals structures of AuNFs could generate strong plasmonic coupling-based optical signals, which greatly improved the detection sensitivity than Au nanoparticles including the short time-dependent, large LSPR peak shift and distinguished color changing. With the increases of ALP activity, the ALP-triggered silver deposition on AuNFs led to a morphology changes and tremendous LSPR peak blue shift accompanied with scattering color changes from red to green. The ability of AuNFs for *in-situ* detection of ALP activity in human serum with a better analytical performances and the cellular ALP activity in response to ALP-based drug treatments were demonstrated. Thus, the proposed method paves a new avenue for cell studies, and hold great potential for discovering novel ALP-based drugs applications.

ASSOCIATED CONTENT

Supporting Information

Additional information as noted in text. This material is available free of charge via the Internet at http://pubs.acs.org.

AUTHOR INFsORMATION

Corresponding Author

E-mail addresses: liusq@seu.edu.cn (S.Q. Liu); Tel.: 86-25-52090613; Fax: 86-25-52090198

Notes

The authors declare no competing financial interest.

ACKNOWLEDGEMENTS

We gratefully appreciate the support from National Natural Science Foundation of China (21635004 and 21627806).

REFERENCES

(1) Kang, E. B.; Choi, C. A.; Mazrad, Z. A. I.; Kim, S. H.; In, I.; Park, S. Y. Determination of Cancer Cell-Based pH-Sensitive Fluorescent Carbon Nanoparticles of Cross-Linked Polydopamine by Fluorescence Sensing of Alkaline Phosphatase Activity on Coated Surfaces and Aqueous Solution. *Anal. Chem.* **2017**, *89*, 13508-13517.

(2) Zhang, H.; Xu, C.; Liu, J.; Li, X.; Guo, L.; Li, X. An Enzyme-Activatable Probe With a Self-Immolative Linker for Rapid and Sensitive Alkaline Phosphatase Detection and Cell Imaging Through a Cascade Reaction. *Chem. Commun.* **2015**, *51,*

7031-7034.

(3) Deng, J.; Yu, P.; Wang, Y.; Mao, L. Real-time Ratiometric Fluorescent Assay for Alkaline Phosphatase Activity with Stimulus Responsive Infinite Coordination Polymer Nanoparticles. *Anal. Chem.* **2015**, *87*, 3080-3086.

(4) Chen, C.; Zhao, J.; Lu, Y.; Sun, J.; Yang, X. Fluorescence Immunoassay Based on the Phosphate-Triggered Fluorescence Turn-on Detection of Alkaline Phosphatase. *Anal. Chem.* **2018**, *90*, 3505-3511.

(5) Chen, L.; Yang, G.; Wu, P.; Cai, C. Real-Time Fluorescence Assay of Alkaline Phosphatase in Living Cells Using Boron-Doped Graphene Quantum Dots as Fluorophores. *Biosens. Bioelectron.* **2017**, *96*, 294-299.

(6) Li, J.; Si, L.; Bao, J.; Wang, Z.; Dai, Z. Fluorescence Regulation of Poly(thymine)-Templated Copper Nanoparticles via an Enzyme-Triggered Reaction Toward Sensitive and Selective Detection of Alkaline Phosphatase. *Anal. Chem.* **2017**, *89*, 3681-3686.

(7) Li, S. J.; Li, C. Y.; Li, Y. F.; Fei, J.; Wu, P.; Yang, B.; Yang, J.; Nie, S. X. Facile and Sensitive Near-Infrared Fluorescence Probe for the Detection of Endogenous Alkaline Phosphatase Activity In Vivo. *Anal. Chem.* **2017**, *89*, 6854-6860.

(8) Gallo, R. L.; Dorschner, R. A.; Takashima, S.; Klagsbrun, M.; Eriksson, E.; Bernfield, M. Endothelial Cell Surface Alkaline Phosphatase Activity is Induced by IL-6 Released During Wound Repair. *J. Invest. Dermatol.* **1997**, *109*, 597-602.

(9) Liu, H. W.; Li, K.; Hu, X. X.; Zhu, L.; Rong, Q.; Liu, Y.; Zhang, X. B.; Hasserodt, J.; Qu, F. L.; Tan, W. In Situ Localization of Enzyme Activity in Live Cells by a

Molecular Probe Releasing a Precipitating Fluorochrome. *Angew. Chem.* **2017**, *129*, 11950-11954.

(10) Dong, L.; Qian, J.; Hai, Z.; Xu, J.; Du, W.; Zhong, K.; Liang, G. Alkaline Phosphatase-Instructed Self-Assembly of Gadolinium Nanofibers for Enhanced T_2-Weighted Magnetic Resonance Imaging of Tumor. *Anal. Chem.* **2017**, *89*, 6922-6925.

(11) Zhan, J.; Cai, Y.; He, S.; Wang, L.; Yang, Z. Tandem Molecular Self-Assembly in Liver Cancer Cells. *Angew. Chem., Int. Ed.* **2018**, *57*, 1813-1816.

(12) Tan, Y.; Zhang, L.; Man, K. H.; Peltier, R.; Chen, G.; Zhang, H.; Zhou, L.; Wang, F.; Ho, D.; Yao, S. Q.; Hu, Y.; Sun, H. Reaction-Based Off−On Near-infrared Fluorescent Probe for Imaging Alkaline Phosphatase Activity in Living Cells and Mice. *ACS appl. Mater. Interfaces.* **2017**, *9*, 6796-6803.

(13) Feng, Z.; Wang, H.; Zhou, R.; Li, J.; Xu, B. Enzyme-Instructed Assembly and Disassembly Processes for Targeting Downregulation in Cancer Cells. *J. Am. Chem. Soc.* **2017**, *139*, 3950-3953.

(14) Liu, H.; Li, M.; Xia, Y.; Ren, X. A Turn-On Fluorescent Sensor for Selective and Sensitive Detection of Alkaline Phosphatase Activity with Gold Nanoclusters Based on Inner Filter Effect. *ACS appl. Mater. Interfaces.* **2016**, *9*, 120-126.

(15 Lakra, S.; J. Jadhav, V.; Garg, S. R. Development of a Chromatographic Method for the Determination of Alkaline Phosphatase Activity in Pasteurized Milk. *Food Anal. Methods* **2016**, *9*, 2002-2009.

(16) Wu, Z.; Zhou, C. H.; Pan, L. J.; Zeng, T.; Zhu, L.; Pang, D. W.; Zhang, Z. L. Reliable Digital Single Molecule Electrochemistry for Ultrasensitive Alkaline

Phosphatase Detection. *Anal. Chem.* **2016**, *88*, 9166-9172.

(17) Xu, L.; Zong, C.; Zheng, X.; Hu, P.; Feng, J.; Ren, B. Label-Free Detection of Native Proteins by Surface-Enhanced Raman Spectroscopy Using Iodide-Modified Nanoparticles. *Anal. Chem.* 2014, *86*, 2238-2245.

(18) Guo, Y.; Wu, J.; Li, J.; Ju, H. A Plasmonic Colorimetric Strategy for Biosensing Through Enzyme Guided Growth of Silver Nanoparticles on Gold Nanostars. *Biosens. Bioelectron.* **2016**, *78*, 267-273.

(19) Li, G.; Fu, H.; Chen, X.; Gong, P.; Chen, G.; Xia, L.; Wang, H.; You, J.; Wu, Y. Facile and Sensitive Fluorescence Sensing of Alkaline Phosphatase Activity with Photoluminescent Carbon Dots Based on Inner Filter Effect. *Anal. Chem.* **2016**, *88*, 2720-2726.

(20) Gao, Z.; Deng, K.; Wang, X. D.; Miró, M.; Tang, D. High-Resolution Colorimetric Assay for Rapid Visual Readout of Phosphatase Activity Based on Gold/Silver Core/Shell Nanorod. *ACS appl. Mater. Interfaces.* **2014**, *6*, 18243-18250.

(21) Liu, M.; Li, Q.; Liang, L.; Li, J.; Wang, K.; Li, J.; Lv, M.; Chen, N.; Song, H.; Lee, J.; Shi, J.; Wang, L.; Lal, R.; Fan, C. Real-time Visualization of Clustering and Intracellular Transport of Gold Nanoparticles by Correlative Imaging. *Nat. commun.* **2017**, *8*, 15646-15646.

(22) Qian, R.; Cao, Y.; Long, Y. T. Dual-Targeting Nanovesicles for In Situ Intracellular Imaging of and Discrimination between Wild-type and Mutant p53. *Angew. Chem., Int. Ed.* **2016**, *55*, 719-723.

(23) Liang, K.; Liu, F.; Fan, J.; Sun, D.; Liu, C.; Lyon, C. J.; Bernard, D. W.; Li, Y.;

Yokoi, K.; Katz, M. H.; Koay, E. J.; Zhao, Z.; Hu, Y. Nanoplasmonic Quantification of Tumour-Derived Extracellular Vesicles in Plasma Microsamples for Diagnosis and Treatment Monitoring. *Nat. biomed. Eng.* **2017**, *1*, 0021-0021.

(24) Sobral-Filho, R. G.; Brito-Silva, A. M.; Isabelle, M.; Jirasek, A.; Lum, J. J.; Brolo, A. G. Plasmonic Labeling of Subcellular Compartments in Cancer Cells: Multiplexing with Fine-Tuned Gold and Silver Nanoshells. *Chem. Sci.* **2017**, *8*, 3038-3046.

(25) Chen, L.; Li, H.; He, H.; Wu, H.; Jin, Y. Smart Plasmonic Glucose Nanosensors as Generic Theranostic Agents for Targeting-Free Cancer Cell Screening and Killing. *Anal. Chem.* **2015**, *87*, 6868-6874.

(26) He, X.; Zhao, Z.; Xiong, L. H.; Gao, P. F.; Peng, C.; Li, R. S.; Xiong, Y.; Li, Z.; Sung, H. H.; Williams, I. D.; Kwok, R. T.; Lam, J. W.; Huang, C. Z.; Ma, N.; Tang, B. Z. Redox-Active AIEgen Derived Plasmonic and Fluorescent Core@shell Nanoparticles for Multimodality Bioimaging. *J. Am. Chem. Soc.* **2018**, *140*, 6904-6911.

(27) Ma, J.; Zhan, L.; Li, R. S.; Gao, P. F.; Huang, C. Z. Color-Encoded Assays for the Simultaneous Quantification of Dual Cancer Biomarkers. *Anal. Chem.* **2017**, *89*, 8484-8489.

(28) Li, X. L.; Zhang, Z. L.; Zhao, W.; Xia, X. H.; Xu, J. J.; Chen, H. Y. Oriented Assembly of Invisible Probes: Towards Single mRNA Imaging in Living Cells. *Chem. Sci.* **2016**, *7*, 3256-3263.

(29) Li, K.; Wang, K.; Qin, W.; Deng, S.; Li, D.; Shi, J.; Huang, Q.; Fan, C.

DNA-Directed Assembly of Gold Nanohalo for Quantitative Plasmonic Imaging of Single-Particle Catalysis. *J. Am. Chem. Soc.* **2015**, *137*, 4292-4295.

(30) Zhao, Y.; He, Y. K.; Zhang, J.; Wang, F. B.; Wang, K.; Xia, X. H. Conformational Change and Biocatalysis-Triggered Spectral Shift of Single Au Nanoparticles. *Chem. Commun.* **2014**, *50*, 5480-5483.

(31) Choi, Y.; Park, Y.; Kang, T.; Lee, L. P. Selective and Sensitive Detection of Metal Ions by Plasmonic Resonance Energy Transfer-Based Nanospectroscopy. *Nat. Nanotechnol*. **2009**, *4*, 742-746.

(32) Zhou, J.; Gao, P. F.; Zhang, H. Z.; Lei, G.; Zheng, L. L.; Liu, H.; Huang, C. Z. Color Resolution Improvement of the Dark-Field Microscopy Imaging of Single Light Scattering Plasmonic Nanoprobes for microRNA Visual Detection. *Nanoscale* **2017**, *9*, 4593-4600.

(33) Nguyen, A. H.; Ma, X.; Sim, S. J. Gold Nanostar Based Biosensor Detects Epigenetic Alterations on Promoter of Real Cells. *Biosens. Bioelectron.* **2015**, *66*, 497-503.

(34) Cheng, H.; Fuku, K.; Kuwahara, Y.; Mori, K.; Yamashita, H. Harnessing Single-Active Plasmonic Nanostructures for Enhanced Photocatalysis Under Visible Light. *J. Mater. Chem. A* **2015**, *3*, 5244-5258.

(35) Olson, J.; Dominguez-Medina, S.; Hoggard, A.; Wang, L. Y.; Chang, W. S.; Link, S. Optical Characterization of Single Plasmonic Nanoparticles. *Chem. Soc. Rev.* **2015**, *44*, 40-57.

(36) Kumar, A.; Kim, S.; Nam, J. M. Plasmonically Engineered Nanoprobes for

Biomedical Applications. *J. Am. Chem. Soc.* **2016**, *138*, 14509-14525.

(37) Shu, J.; Qiu, Z.; Lv. S.; Zhang, K.; Tang, D. Plasmonic Enhancement Coupling with Defect-Engineered TiO_{2-x}: A Mode for Sensitive Photoelectrochemical Biosensing. *Anal. Chem.* **2018**, *90*, 2425-2429.

(38) Zhuang, J.; Lai, W.; Xu, M.; Zhou, Q.; Tang, D. Plasmonic AuNP/g-C_3N_4 Nanohybrid-Based Photoelectrochemical Sensing Platform for Ultrasensitive Monitoring of Polynucleotide Kinase Activity Accompanying DNAzyme-Catalyzed Precipitation Amplification. *ACS appl. Mater. Interfaces.* **2015**, *7*, 8330-8338.

(39) Tsoulos, T. V.; Han, L.; Weir, J.; Xin, H. L.; Fabris, L. A Closer Look at the Physical and Optical Properties of Gold Nanostars: An Experimental and Computational Study. *Nanoscale* **2017**, *9*, 3766-3773.

(40) Zhang, Y.; Shuai, Z.; Zhou, H.; Luo, Z.; Liu, B.; Zhang, Y.; Zhang, L.; Chen, S.; Chao, J.; Weng, L.; Fan, Q.; Fan, C.; Huang, W.; Wang, L. Single-Molecule Analysis of MicroRNA and Logic Operations Using a Smart Plasmonic Nanobiosensor. *J. Am. Chem. Soc.* **2018**, *140*, 3988-3993.

(41) Xiong, B.; Zhou, R.; Hao, J.; Jia, Y.; He, Y.; Yeung, E. S. Highly Sensitive Sulphide Mapping in Live Cells by Kinetic Spectral Analysis of Single Au-Ag Core-Shell Nanoparticles. *Nat. commun*. **2013**, *4*, 1708-1708.

(42) Wang, K.; Shangguan, L.; Liu, Y.; Jiang, L.; Zhang, F.; Wei, Y.; Qi, Z.; Wang, K.; Liu, S. In Situ Detection and Imaging of Telomerase Activity in Cancer Cell Lines via Disassembly of Plasmonic Core-Satellites Nanostructured Probe. *Anal. Chem.* **2017**, *89*, 7262-7268.

(43) Chen, Z.; Li, J.; Chen, X.; Cao, J.; Zhang, J.; Min, Q.; Zhu, J. J. Single Gold@Silver Nanoprobes for Real-Time Tracing the Entire Autophagy Process at Single-Cell Level. *J. Am. Chem. Soc.* **2015**, *137*, 1903-1908.

(44) Li, M. X.; Xu, C. H.; Zhang, N.; Qian, G. S.; Zhao, W.; Xu, J. J.; Chen, H. Y. Exploration of the Kinetics of Toehold-Mediated Strand Displacement via Plasmon Rulers. *ACS nano* **2018**, *12*, 3341-3350.

(45) Kumar, A.; Kumar, S.; Rhim, W. K.; Kim, G. H.; Nam, J. M. Oxidative Nanopeeling Chemistry-Based Synthesis and Photodynamic and Photothermal Therapeutic Applications of Plasmonic Core-Petal Nanostructures. *J. Am. Chem. Soc.* **2014**, *136*, 16317-16325.

(46) Liu, J.; Lu, Y. Preparation of Aptamer-Linked Gold Nanoparticle Purple Aggregates for Colorimetric Sensing of Analytes. *Nat. Protoc.* **2006**, *1*, 246-252.

(47) Brown, K. R.; Natan, M. J. Hydroxylamine Seeding of Colloidal Au Nanoparticles in Solution and on Surfaces. *Langmuir* **1998**, *14*, 726-728.

(48) Zhang, X.; Gouriye, T.; Göeken, K.; Servos, M. R.; Gill, R.; Liu, J. Toward Fast and Quantitative Modification of Large Gold Nanoparticles by Thiolated DNA: Scaling of Nanoscale Forces, Kinetics, and the Need for Thiol Reduction. *J. Phys. Chem. C* **2013**, *117*, 15677-15684.

(49) Zhou, J.; Xiong, Q.; Ma, J.; Ren, J.; Messersmith, P. B.; Chen, P.; Duan, H. Polydopamine-Enabled Approach toward Tailored Plasmonic Nanogapped Nanoparticles: From Nanogap Engineering to Multifunctionality. *ACS nano* **2017**, *10*, 11066-11075.

(50) Wang, J. G.; Hua, X.; Li, M.; Long, Y. T. Mussel-Inspired Polydopamine Functionalized Plasmonic Nanocomposites for Single-Particle Catalysis. *ACS appl. Mater. Interfaces.* **2017**, *9*, 3016-3023.

Figure captions

Figure 1. (A) UV-*vis* spectra and photographs (inset) of AuNPs and AuNFs. (B) LSPR spectrum, (C) TEM images and (D) corresponding scattering color (right side) of an individual AuNPs, AuNFs and AuNF@Ag. The AuNF@Ag was generated by incubation of AuNFs in 10 mM pH 8.5 Tris buffer containing 0.01 μM $AgNO_3$, 0.02 μM AAP and 60 μU L^{-1} of ALP for 30min.

Scheme 1. Schematic illustration of AuNFs probe for *in-situ* detection of ALP activity.

Figure 2. (A) Dark-field images and corresponding scattering spectra of an individual AuNFs incubated with 0.01 μM $AgNO_3$, 0.02 μM AAP and ALP activity with (a) 0.1, (b) 0.5, (c) 1, (d) 5, (e) 10, (f) 30, (g) 60 and (h) 80 μU L^{-1} for 30min. (B) Plot of the LSPR peak shifts of AuNFs *vs* ALP activity. Inset: linear relationship at ALP activity range from 0.1 μU L^{-1} to 60 μU L^{-1}.

Figure 3. (A) Time-dependent of the LSPR peak shifts for AuNFs and AuNPs incubation in 10 mM pH 8.5 Tris buffer containing 0.01 μM $AgNO_3$, 0.02 μM AAP and 60 μU L^{-1} of ALP, respectively. (B) Dose-dependent of the LSPR peak shifts for AuNFs and AuNPs incubation in 10 mM pH 8.5 Tris buffer containing 0.01 μM $AgNO_3$, 0.02 μM AAP and various concentrations of ALP for 30 min, respectively. (C) Selectivity of the ALP sensing strategy. Here, 5 μU L^{-1} of ALP, 100 ng L^{-1} of bovine serum albumin (BSA), thrombin (Thr), glucose oxidase (GOX), and glucose dehydrogenase (GDH), respectively, were incubated with a mixture solution in 10 mM pH 8.5 Tris buffer containing AuNFs, 0.01 μM $AgNO_3$ and 0.02 μM AAP for 30 min. (D) Inhibition effect of Na_3VO_4 on ALP activity. Na_3VO_4 with different

concentration were added to 10 mM pH 8.5 Tris buffer containing AuNFs, 0.01 μM $AgNO_3$ and 0.02 μM AAP and incubated for 30 min.

Figure 4. Dark-field images after HepG2 incubated with 0.25 pM AuNFs, it was further incubated with 2.5 nM $AgNO_3$, 5 nM AAP in 10 mM pH 8.5 Tris buffer for (A) 0 min, (B) 10 min, (C) 20 min, and (D) 30 min. (E) The corresponding LSPR spectrum of the selected three probes on the cell varied with time. (F) The LSPR peak shifts depended on incubation times for 10, 20, 30 min.

Figure 5. Dark-field images of (A) HepG2 incubation with 0.25 pM AuNFs and (B) After HepG2 incubated with AuNFs, it was further incubated with 2.5 nM $AgNO_3$, 5 nM AAP in 10 mM pH 8.5 Tris buffer for 30 min; (C) Hek293 incubation with 0.25 pM AuNFs and (D) After Hek293 incubated with AuNFs, it was further incubated with 2.5 nM $AgNO_3$, 5 nM AAP in 10 mM pH 8.5 Tris buffer for 30 min. Dark-field images and corresponding scattering spectra after HepG2 incubation with (E, F) 0 nM, (G, H) 20 nM, (I, J) 100 nM, (K, L) 200 nM Na_3VO_4, and 0.25 pM AuNFs, it was further incubated without (E, G, I, K) and with (F, H, J, L) 2.5 nM $AgNO_3$, 5 nM AAP in 10 mM pH 8.5 Tris buffer for 30 min.

Figure 1

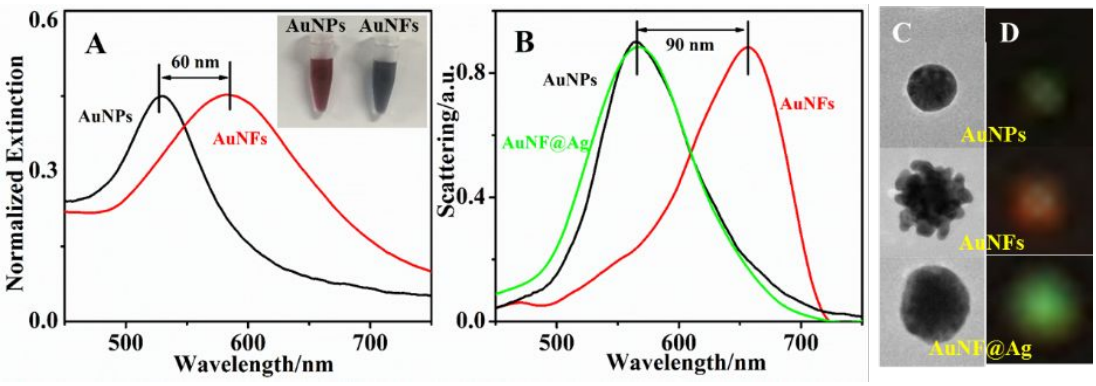
A
60 nm
AuNPs
AuNFs
AuNPs AuNFs
Normalized Extinction
0.6
0.3
0.0
500
600
700
Wavelength/nm
B
90 nm
AuNPs
AuNF@Ag
AuNFs
Scattering/a.u.
0.8
0.4
0.0
500
600
700
Wavelength/nm
C
D
AuNPs
AuNFs
AuNF@Ag

Scheme 1

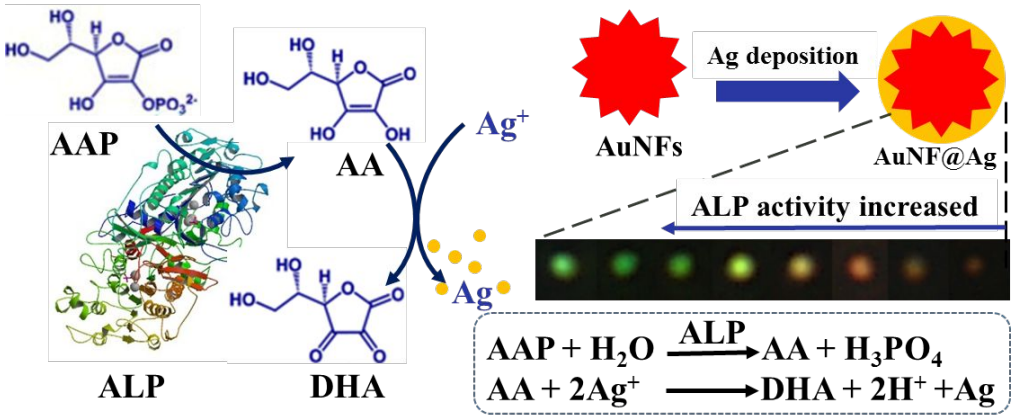
AAP
ALP
AA
DHA
Ag+
Ag
AuNFs
Ag deposition
AuNF@Ag
ALP activity increased
AAP + H2O ALP AA + H3PO4
AA + 2Ag+ DHA + 2H+ +Ag

Figure 2

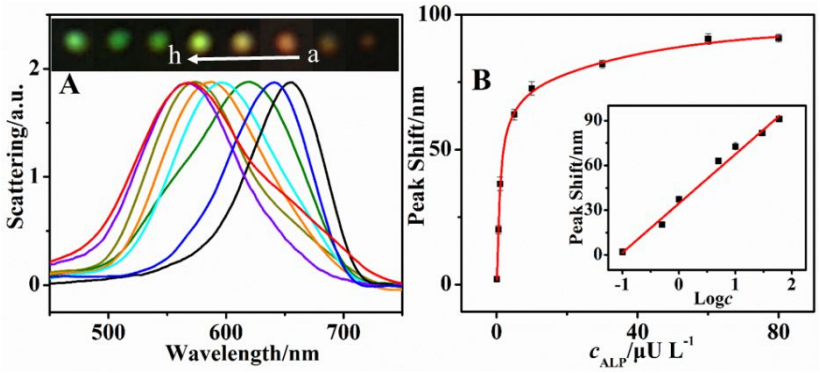
h
a
A
Scattering/a.u.
Wavelength/nm
B
Peak Shift/nm
c_{ALP}/μU L^{-1}
Peak Shift/nm
Logc

Figure 3

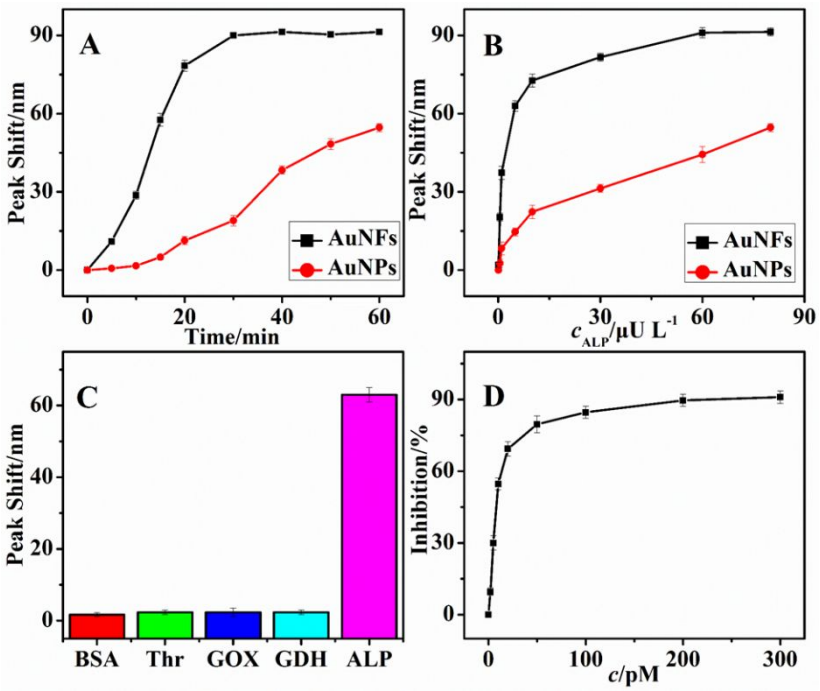
A
Peak Shift/nm
Time/min
AuNFs
AuNPs
B
Peak Shift/nm
c_{ALP}/μU L^{-1}
AuNFs
AuNPs
C
Peak Shift/nm
BSA
Thr
GOX
GDH
ALP
D
Inhibition/%
c/pM

Figure 4

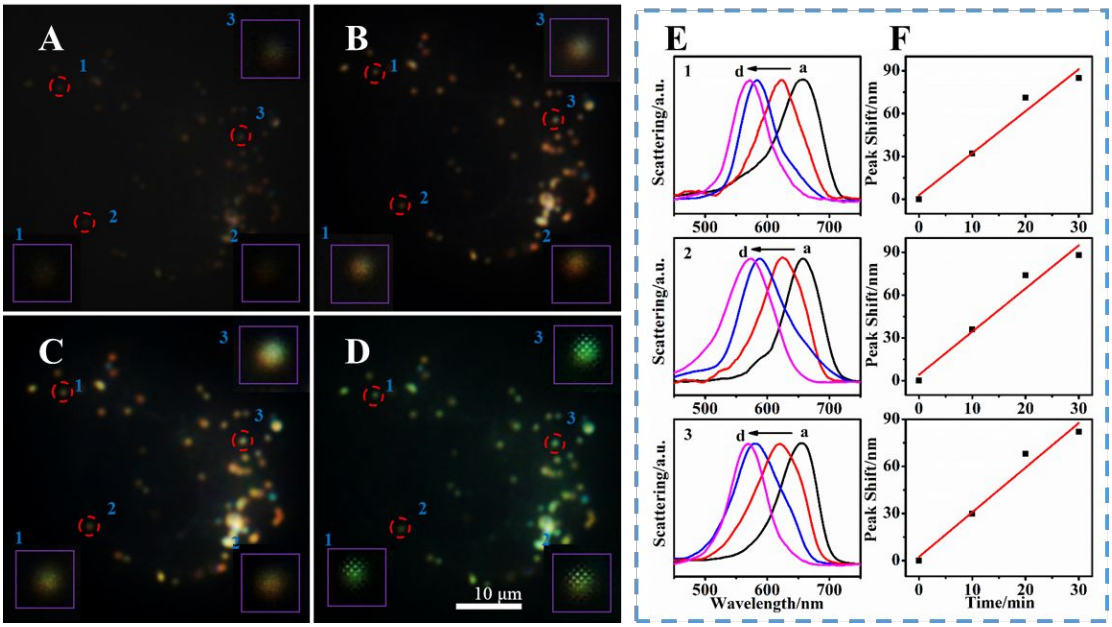
A
B
C
D
E
F
10 μm
Scattering/a.u.
Wavelength/nm
Peak Shift/nm
Time/min
d
a

Figure 5

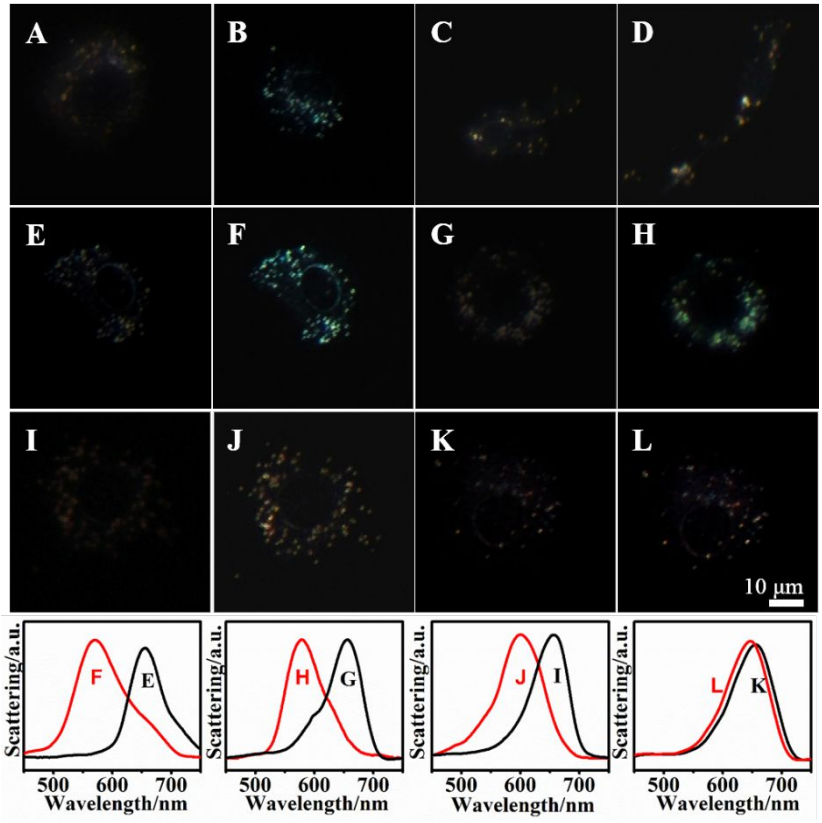
A
B
C
D
E
F
G
H
I
J
K
L
10 μm
Scattering/a.u.
F
E
H
G
J
I
L
K
500 600 700
Wavelength/nm

For TOC only

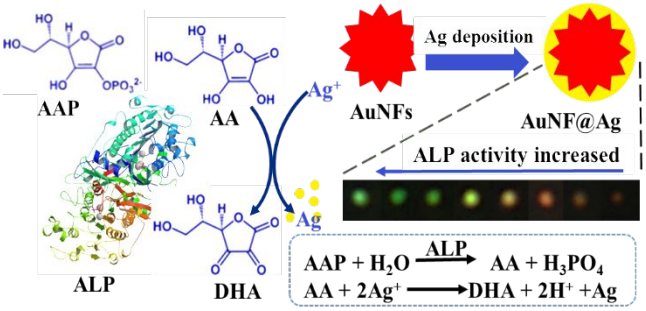
AAP
AA
Ag+
AuNFs
Ag deposition
AuNF@Ag
ALP activity increased
Ag
ALP
DHA
AAP + H2O ALP AA + H3PO4
AA + 2Ag+ DHA + 2H+ +Ag